

Multifunctional SBA-15 for magnetically oriented and pH targeted delivery of ibuprofen

H. M. Lin, R. Xing, X. Wu, P. P. Jiang, J. J. Jiang and F. Y. Qu*

A magnetic and pH targeting drug delivery system based on the magnetic nanocomposite doping mesoporous silica material has been successfully prepared. The material exhibited highly ordered mesostructure, large Brunauer–Emmett–Teller surface area, high pore volume, regular nanoparticle morphology and superior magnetic property. The structure and properties of the magnetic mesoporous nanocomposites were characterised by X-ray diffraction, scanning electron microscope, transmission electron microscope, N₂ adsorption–desorption, Fourier transform infrared spectroscopy and vibrating sample magnetometer technique. The as obtained magnetic mesoporous material was used as drug carrier, and ibuprofen was used as model drug. The releases in simulated proximal intestine fluid (pH 7.4) and simulated gastric fluid (pH 1.2) were studied. Therefore, a novel multifunctional drug delivery system with magnetically oriented and alkalescence site targeted release has been obtained.

Keywords: SBA-15, Magnetically oriented, pH targeted, Drug release

Introduction

Among the various types of drug delivery systems, biocompatible inorganic mesoporous silica nanoparticles (MSNs) have attracted much attention in the biomedical research field. With unique properties such as tunable pore size and structure, large surface areas and pore volumes, controllable morphology and chemically modifiable surfaces and high chemical and thermal stabilities, MSNs have supreme potential application in the biomedical field, such as cell markers for magnetic resonance imaging and optical imaging^{1–6} and as carriers for various guest molecules with therapeutic efficacy (e.g. proteins,⁷ anticancer drugs,⁸ genes,^{9,10} antibiotics, non-steroidal anti-inflammatory drugs,¹¹ etc.). As known, conventional pure MSNs (e.g. MCM-41 and SBA-15) are unintelligent materials, and drug cannot be released in a controllable manner to precisely match the actual physiological needs at the proper time/site, which may decrease bioavailability, increase toxicity effects and affect clinical therapeutic efficiency.

To overcome this disadvantage, one strategy is to fabricate stimuli responsive or 'smart' drug carrier system by the functionalisation of the MSNs and to make them thermoresponsive, pH responsive, light sensitive, magnetism sensitive, etc. The system can be sensitive to physiological or external conditions (e.g. pH, temperature, light and magnetism) and accordingly delivers the necessary amount of drug in response to stimuli–response

in a controlled manner. So far, several research groups have made great efforts to explore such drug carrier systems. Xu *et al.* reported a pH controlled drug release system prepared by coating pH sensitive polymer hydroxypropyl methylcellulose phthalate on drug loaded mesoporous SBA-15 tablet. This composite system showed intelligent performance in the aspect of drug release.¹² Liu *et al.* reported magnetic mesoporous silica microspheres with thermosensitive polymer shell for controlled drug release, and the drug release behaviour was dependent on the temperature and had a close correlation with the volume phase transition temperature.¹³ Lin *et al.* reported light sensitive intelligent mesoporous bioactive glass for drug delivery. Irradiation with UV light (>310 nm) induced photodimerisation of the coumarin modified MBG, which led to the pores' closing with cyclobutane dimers and trapping of the guest phenanthrene in the mesopores.¹⁴

As we know, the superparamagnetic properties of the magnetic nanoparticles (such as γ -Fe₂O₃ and Fe₃O₄) are of great interest for drug delivery. They can carry the drugs and be guided to the targeted organs or locations inside the body, which will facilitate the therapeutic efficiency and avoid the damage of normal organs or tissues before targeting the desired positions due to drug toxicity. Zhu *et al.* reported a self-templating method for the assembly of unique core/cell superparamagnetic iron oxide/carbon porous materials, in which the magnetic nanoparticles were enveloped by a carbon layer from hybrid core/shell materials.¹⁵ Zhu *et al.* reported rattle type Fe₃O₄/SiO₂ hollow mesoporous spheres with large cavities by using colloidal carbon spheres as templates.¹⁶

Generally, magnetic mesoporous silica nanocomposites could be synthesised according to the following two approaches: first, coating a mesoporous silica shell

Key Laboratory of Design and Synthesis of Functional Materials and Green Catalysis, Universities of Heilongjiang Province and College of Chemistry and Chemical Engineering, Harbin Normal University, Harbin 150025, China

*Corresponding author, email qufengyu2010@yahoo.cn

around the magnetic nanoparticles to form a magnetic (core)/silica (shell) structure¹⁷ and second, mixing the metal (ion, nickel, cobalt, etc.) source into the pore of the mesoporous materials by one or two steps and then oxidation/pyrolysis to obtain the magnetic particle doping mesoporous materials.¹⁸ The first method could be used to keep well superparamagnetism of the materials, but it is difficult to obtain nanocomposites with well ordered mesostructure. Moreover, the process was very complex and refractory. However, the materials obtained by the second method possess not only well superparamagnetism but also large surface area/pore volumes and uniform magnetic particles.

Herein, magnetic mesoporous nanocomposites with regular nanoparticle morphologies and good properties were prepared successfully by a facile, low cost, two-step and sol-gel method. The key of our aims is to observe the release behaviours of ibuprofen (IBU) from these magnetic mesoporous nanocomposites in simulated intestine fluid (SIF; pH 1.2) and simulated gastric fluid (SGF; pH 7.4). Furthermore, the influence of the amount of iron for the drug release in different pH media is also discussed.

Experimental

Materials

All the chemicals were purchased from commercial source and used as received without further purification: triblock polyethylene oxide-propylene oxide block copolymer (P123; average molecular weight, 5800; Aldrich), tetraethyl orthosilicate (Tiantai Chemical Co., Tianjin, China), $\text{Fe}(\text{NO}_3)_3 \cdot 9\text{H}_2\text{O}$ (Guangfu Industry of Fine Chemicals Institute, Tianjin, China), ethylene glycol (Bodi Chemical Co., Tianjin, China), HCl (Guangfu Industry of Fine Chemicals Institute), N-hexane (Guangfu Industry of Fine Chemicals Institute) and IBU (Tianzunzezhong Chemical Co., Nanjing).

Preparation of silica samples

The mesoporous silica SBA-15 was synthesised with the use of P123 as the surfactant according to the published reports.¹⁹⁻²¹ Briefly, 4 g of surfactant P123 was dissolved in a mixture of 120 g of water and 60 g of 2M HCl, followed by dropping addition of 8.5 g of tetraethyl orthosilicate. The mixture was stirred for 5 min and then kept at 35°C for 20 h. Later, the mixture was transferred to an autoclave to be heated at 100°C for 24 h. Finally, the sample was collected by filtration, washed with abundant distilled water, dried and calcined at 550°C for 6 h.

Preparation of magnetic mesoporous nanocomposites by sol-gel method

The mesoporous silica SBA-15 was first added into a solution of iron nitrate in ethanol. After stirring at room temperature for 2 h, the mixture was dried at 80°C for 2 h. Then, the sample was impregnated with ethylene glycol up to incipient wetness (per 0.45 g SBA-15 and ~1 mL ethylene glycol). The impregnated sample was heated from room temperature to 350°C with the rate of 2°C min⁻¹ and maintained at 350°C for 3 h in N₂ atmosphere, resulting in the formation of Fe₂O₃/SBA-15 composites. The samples with 10.55 and 25.00 wt-%Fe content were named as Fe₂O₃/SBA-15-1 and Fe₂O₃/SBA-15-2 respectively.

Characterisation

Samples were characterised by scanning electron microscopy (SEM) that was performed using a Hitachi S-4800 operating at an accelerating voltage of 20 kV; affiliated SEM-EDS was used to analyse the sample elements. X-ray diffraction (XRD) data is characterised using a Siemens D5005 diffractometer with Cu K_α radiation at 40 kV and 30 mA. The isotherms of N₂ adsorption/desorption were measured at the temperature of liquid nitrogen using a Micromeritics ASAP 2010M system. The pore size distributions were calculated from the adsorption branches of the N₂ adsorption isotherms using the Barrett-Joyner-Halenda model. A Fourier transform infrared (FTIR) spectroscopy spectrometer (JASCO/IR-420) was used to record the infrared spectra of mesoporous materials. The morphology of the powders was examined by SEM (Hitachi S-4800) and TEM (Hitachi H-8100). Ultraviolet-visible (UV-vis) spectra were taken on a Lambda 45 spectrophotometer. The magnetic measurements were carried out on a vibrating sample magnetometer (Lake Shore, Model 7410).

Drug loading and release *in vitro*

Typically, 0.206 g of Fe₂O₃/SBA-15 sample was suspended in a 10 mL hexane (A.R.) solution of IBU with a concentration of 0.1M at room temperature under stirring for 4 h in a sealed vial to prevent the evaporation of hexane. The drug loading mesoporous materials were recovered by vacuum filtration and dried at room temperature. One millilitre of filtrate was extracted and properly diluted. Then, it was analysed by UV-vis spectroscopy at a wavelength of 220 nm to determine the drug loading.

The obtained samples were compressed into tablets under 4 MPa with a diameter of 10 mm and a thickness of 1 mm for the drug release experiment. The release rate was obtained by soaking the drug loading tablets in 300 mL of SIF and SGF, maintained at 36.7°C respectively. Then, 3.0 mL release medium was removed for analysis at the given intervals with a syringe, and the same volume of fresh release medium was added. The release medium was filtered with syringe filters (0.45 μm). The clear solution without nanospheres was used to estimate the concentration of drug release and was properly diluted and analysed for IBU content at 220 nm using a UV-vis spectrophotometer. Calculation of the corrected concentration of the released IBU is based on the following equation

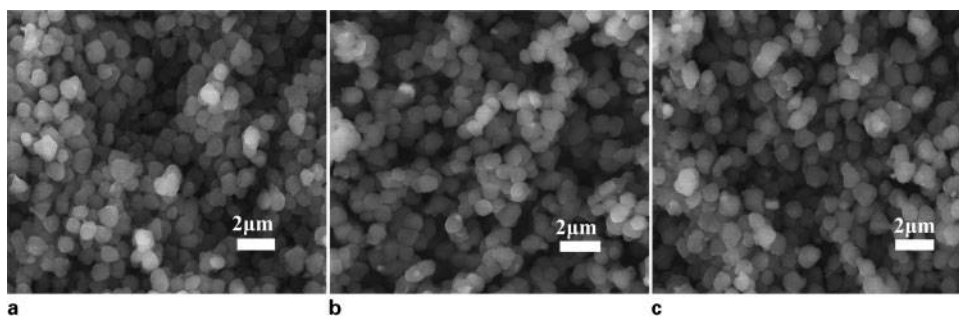
$$C_c = C_t + \frac{v}{V} \sum_0^{t-1} C_t$$

where C_c is the corrected concentration at time t , C_t is the apparent concentration at time t , v is the volume of sample taken and V is the total volume of release fluids.

Results and discussion

Structural characteristics of samples

The morphologies of the nanocomposites are shown in the SEM images (Fig. 1). Pure SBA-15 exhibits uniform spherical particles with a diameter of 0.5 μm from the image (Fig. 1a). After being doped with the magnetic materials, the Fe₂O₃ particles formed on the surface and in the pore of SBA-15. However, the morphologies of Fe₂O₃/SBA-15-1 and Fe₂O₃/SBA-15-2 do not change,



1 Images (SEM) of a SBA-15, b $\text{Fe}_2\text{O}_3/\text{SBA-15-1}$ and c $\text{Fe}_2\text{O}_3/\text{SBA-15-2s}$

and both exhibit uniform spherical particle morphology (Fig. 1b and c). After suitable treatment by hydrofluoric acid, the component of magnetic mesoporous materials is calculated from the data of inductively coupled plasma. By calculating from the results of inductively coupled plasma, the contents of Fe element are 10.55 and 25.00% for $\text{Fe}_2\text{O}_3/\text{SBA-15-1}$ and $\text{Fe}_2\text{O}_3/\text{SBA-15-2}$ respectively.

Figure 2a shows the small angle powder XRD patterns of SBA-15, $\text{Fe}_2\text{O}_3/\text{SBA-15-1}$ and $\text{Fe}_2\text{O}_3/\text{SBA-15-2}$. From Fig. 2a (curve a), SBA-15 shows three peaks indexed as (100), (110) and (200), suggesting a well ordered two-dimensional hexagonal mesostructure, which is in accordance with the other reports.^{22,23} From Fig. 2a (curves b and c), $\text{Fe}_2\text{O}_3/\text{SBA-15-1}$ and $\text{Fe}_2\text{O}_3/\text{SBA-15-2}$ still possess ordered hexagonal mesoporous structure, but the peaks shift to the wide angle compared with SBA-15. According to the Bragg equation: $2d\sin\theta = n\lambda$, the larger diffraction angle of $\text{Fe}_2\text{O}_3/\text{SBA-15}$ results from the smaller interplanar spacing of $\text{Fe}_2\text{O}_3/\text{SBA-15}$. This proves the formation of iron oxide nanoparticles in the pore of SBA-15. Figure 2b shows the wide angle powder XRD patterns of $\text{Fe}_2\text{O}_3/\text{SBA-15-1}$ and $\text{Fe}_2\text{O}_3/\text{SBA-15-2}$. From the diffraction peak positions and relative intensities of the samples, it can be ascribed to the diffraction characteristic peaks of iron oxide spinel (30.4, 35.7, 43.4, 53.8, 57.4 and 63.0°). This is a direct evidence for the formation of magnetic iron oxide particles.

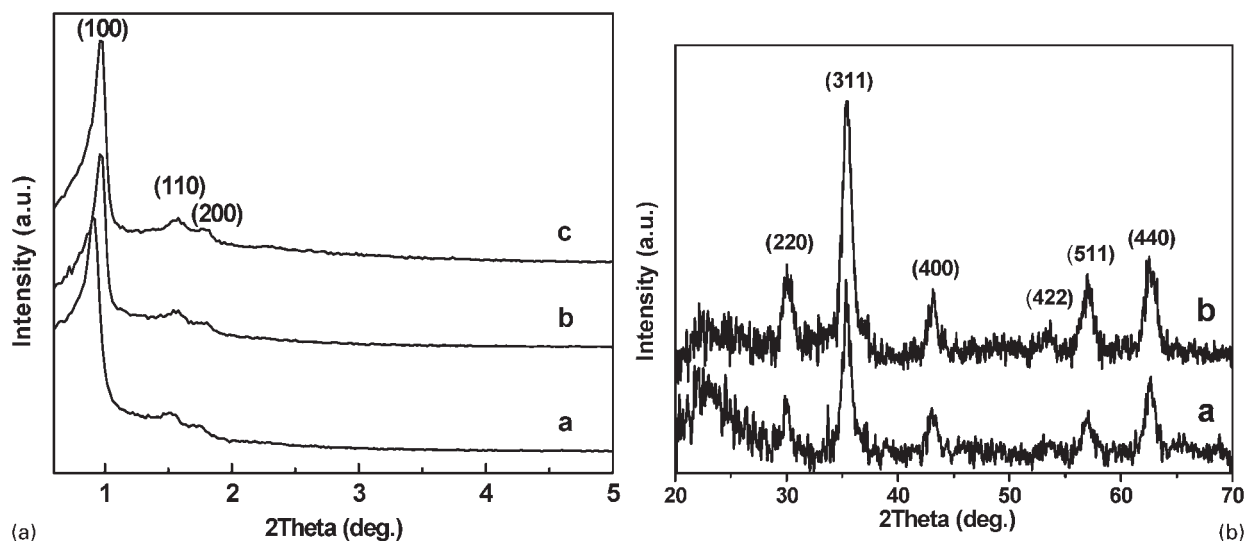
From the TEM images (obtained by scanning photographic negative) of the materials (Fig. 3), highly ordered

two-dimensional hexagonal mesoporous channels can be clearly observed. These TEM images further confirm that the samples possess an ordered mesoporous structure that corresponds to the result of XRD.

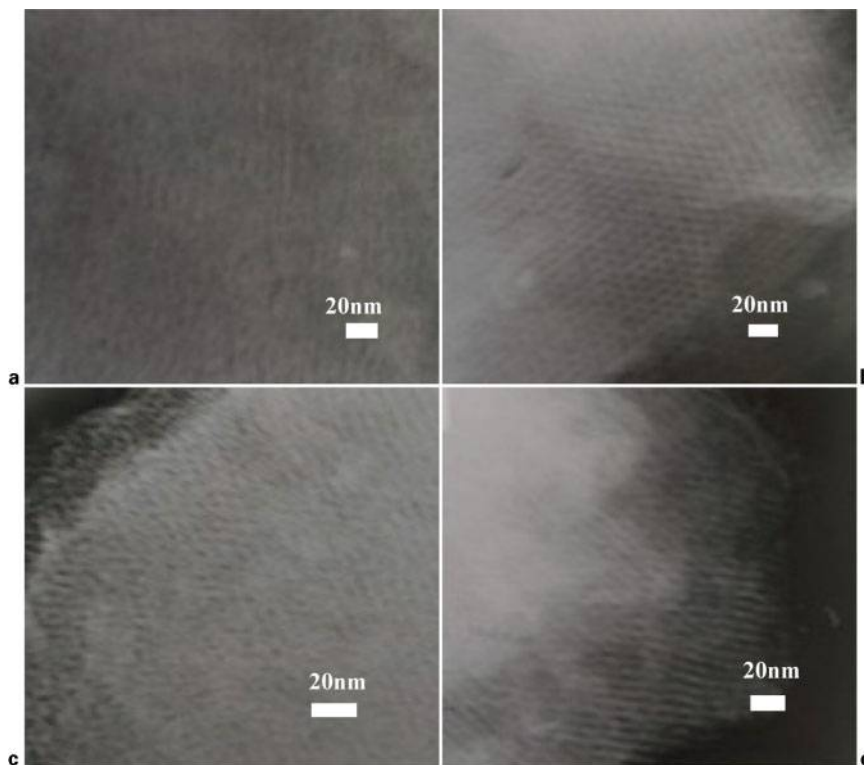
Nitrogen adsorption-desorption and pore size of the three samples are shown in Fig. 4. All the samples show the type IV isotherm²⁴ for mesoporous structure. From the images, it can be found that with the increase in the content of iron, the adsorption amount of the samples decreases obviously. It proves that the formation of iron oxide nanoparticles in the pore also increases with the iron content increases, and the surface area, pore volume and pore diameter of the materials also decrease with the increase in content of iron (Table 1), which also testify the formation of iron oxide nanoparticles inside the pores of the silica.

Magnetic characterisation of magnetic mesoporous nanocomposites

The magnetisation reversal process of magnetic samples was characterised by a vibrating sample magnetometer at room temperature (Table 2 and Fig. 5). No hysteresis loops are observed from the magnetisation curves (Fig. 5), and this confirms the superparamagnetic behaviour of the synthesised samples. The saturation magnetisation M_s values for $\text{Fe}_2\text{O}_3/\text{SBA-15-1}$ and $\text{Fe}_2\text{O}_3/\text{SBA-15-2}$ shown in Table 2 are 3.2714 and 6.8667 emu g^{-1} respectively. It is shown that with the increase in the formation of iron oxide nanoparticles, the value of saturation magnetisation M_s enhances. The low value of M_r , close to zero, indicates

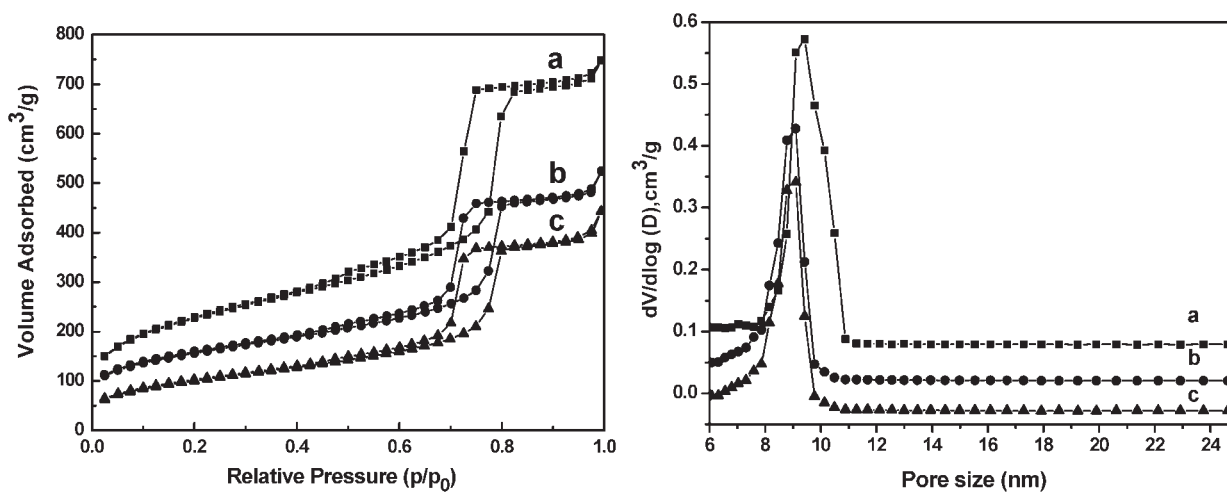


2 a low angle of XRD of SBA-15 (curve a), $\text{Fe}_2\text{O}_3/\text{SBA-15-1}$ (curve b) and $\text{Fe}_2\text{O}_3/\text{SBA-15-2}$ (curve c) and b wide angle of XRD of $\text{Fe}_2\text{O}_3/\text{SBA-15-1}$ (curve a) and $\text{Fe}_2\text{O}_3/\text{SBA-15-2}$ (curve b)



a, b Fe₂O₃/SBA-15-1; c, d Fe₂O₃/SBA-15-2

3 Images (TEM) obtained by scanning photographic negative of Fe₂O₃/SBA-15



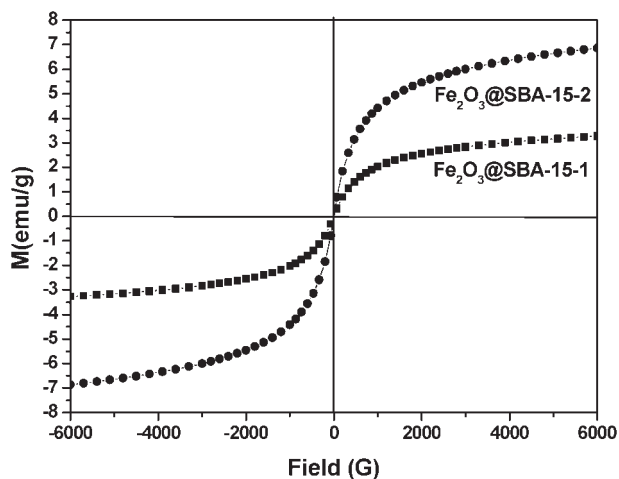
4 Nitrogen sorption isotherm and pore size of SBA-15 (curve a), Fe₂O₃/SBA-15-1 (curve b) and Fe₂O₃/SBA-15-2 (curve c)

Table 1 Brunauer–Emmett–Teller (BET) surface area, pore volume and average diameter of samples

Sample	BET surface area/m ² g ⁻¹	Pore volume/cm ³ g ⁻¹	Pore diameter/nm	IBU/wt-%
SBA-15	820	1.08	9.2	30.33
Fe ₂ O ₃ /SBA-15-1	426	0.70	9.0	28.91
Fe ₂ O ₃ /SBA-15-2	366	0.63	8.8	28.16

Table 2 Magnetic parameters of different samples

Sample	Coercivity H _c /G	Remanent magnetisation M _r /emu g ⁻¹	Saturation magnetisation M _s /emu g ⁻¹
Fe ₂ O ₃ /SBA-15-1	73.128 × 10 ⁻³	347.80 × 10 ⁻⁶	3.2714
Fe ₂ O ₃ /SBA-15-2	0.50224	5.9345 × 10 ⁻³	6.8667



5 Magnetisation curves of $\text{Fe}_2\text{O}_3/\text{SBA-15-1}$ and $\text{Fe}_2\text{O}_3/\text{SBA-15-2}$

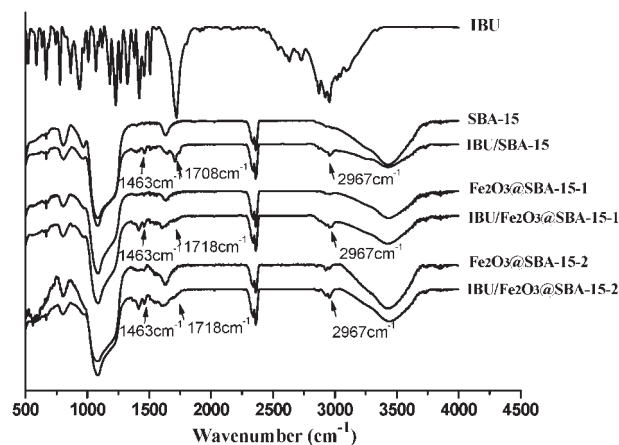
that the prepared samples exhibit superparamagnetic behaviours at room temperature.²⁵ Photographs of the black particle separation process are shown in Fig. 6, which indicated that the materials can be introduced by the magnet. Therefore, they may be used in targeted drug delivery and separation by means of an external magnetic field to achieve the purpose of local treatment.

Drug loading and release profiles

The drug loading capacities of SBA-15 and magnetic SBA-15 are shown in Table 1. SBA-15/IBU has the highest loading amount of 30.33 wt-% due to the highest BET surface area ($820 \text{ m}^2 \text{ g}^{-1}$). Infrared spectra of the drug loaded samples further gave a direct demonstration of loading IBU in the mesoporous materials. The FTIR spectra of the three samples before and after loaded drugs are shown in Fig. 7. The quaternary carbon atom peaks at 1463 and 1509 cm^{-1} and the alkyl group peaks at 2864 and 2967 cm^{-1} of the loaded samples could be clearly observed,²⁶ which confirms that the IBU has been loaded in the pore of the mesoporous silica system. The characteristic absorption peaks of ν (COOH) at 1725 cm^{-1} and δ_{oop} (OH) at 950 cm^{-1} of IBU are shown in the image, obviously. Meanwhile, the peak of -COOH is at 1708 cm^{-1} for SBA-15/IBU, while it shifts to 1718 cm^{-1} for IBU/ $\text{Fe}_2\text{O}_3/\text{SBA-15}$. The -COOH peak of the drug loading system has a slight blue shift, indicating the interaction between -COOH and the host.

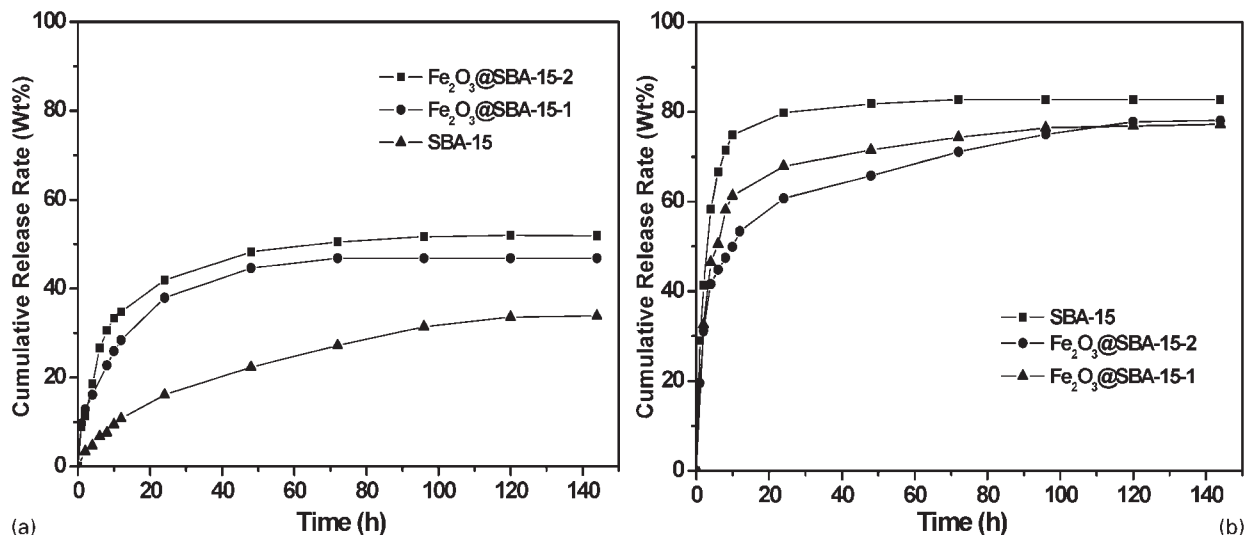


6 Photograph showing ability of IBU/ $\text{Fe}_2\text{O}_3/\text{SBA-15}$ to be magnetically guided



7 Spectra (FTIR) of neat mesoporous silica samples and drug loaded mesoporous silica samples

Figure 8 shows the release behaviour of IBU from the different materials in SGF and SIF over 120 h at 36.7°C respectively. In relation to the release of IBU in SGF (Fig. 8a), it can be seen that pure SBA-15 has a lower release rate and release amount than that of $\text{Fe}_2\text{O}_3/\text{SBA-15-1}$ and $\text{Fe}_2\text{O}_3/\text{SBA-15-2}$, and the release rate and release amount of $\text{Fe}_2\text{O}_3/\text{SBA-15-2}$ are both higher compared with $\text{Fe}_2\text{O}_3/\text{SBA-15-1}$. At last, the final release amounts of SBA-15, $\text{Fe}_2\text{O}_3/\text{SBA-15-1}$ and $\text{Fe}_2\text{O}_3/\text{SBA-15-2}$ in SGF are 33.8, 46.8 and 52.1% respectively. Large quantities of Si-OH are distributed on the surface of SBA-15 and pore, while there are also iron oxide nanoparticles on the surface of $\text{Fe}_2\text{O}_3/\text{SBA-15}$ and pore besides Si-OH. The result is caused by the stronger interaction between -COOH of IBU and -OH of SBA-15 than that between -COOH and Fe of $\text{Fe}_2\text{O}_3/\text{SBA-15}$ in acid medium. However, Fig. 8b shows that the release rate of $\text{Fe}_2\text{O}_3/\text{SBA-15}$ is slower than that of SBA-15 in SIF (pH 7.4). When it releases ~ 4 h, pure SBA-15 has been released $\sim 58.4\%$, while $\text{Fe}_2\text{O}_3/\text{SBA-15-1}$ and $\text{Fe}_2\text{O}_3/\text{SBA-15-2}$ have been released only about 46.3 and 41.7% respectively. When it releases about 10 h, the pure SBA-15 has been released about 75.1%, while $\text{Fe}_2\text{O}_3/\text{SBA-15-1}$ and $\text{Fe}_2\text{O}_3/\text{SBA-15-2}$ have been released about 61.4 and 49.9%. After 48 h, the release of pure SBA-15 has been released completely, but the release of $\text{Fe}_2\text{O}_3/\text{SBA-15-1}$ and $\text{Fe}_2\text{O}_3/\text{SBA-15-2}$ has been until 120 h. At last, the final release amounts of SBA-15, $\text{Fe}_2\text{O}_3/\text{SBA-15-1}$ and $\text{Fe}_2\text{O}_3/\text{SBA-15-2}$ in SIF are 82.7, 76.9 and 78.1% respectively. It is because the IBU (pK_a , 4.7) molecule is deprotonated at pH 7.4. The coordination bond between -COO^- of IBU and Fe of $\text{Fe}_2\text{O}_3/\text{SBA-15}$ is stronger than the hydrogen bond between IBU and silanol, which results in lower release rate and release amount of $\text{Fe}_2\text{O}_3/\text{SBA-15}$ than those of pure SBA-15. In addition, compared with pure SBA-15, the smaller pore diameter and BET surface area of magnetic materials also decrease the release rate. The magnetic material targeting drug delivery system exhibits better controlled release property than pure mesoporous material. In contrast with the release curves in SIF, the cumulate release amount of all samples in SGF is higher because of the lower solubility of IBU in acid medium. Therefore, the magnetic materials have efficacy both on magnetically targeting release and prolonging medicine expiry.



8 Cumulative release rates of IBU in simulated a gastric fluid and b proximal intestine fluid

Conclusions

In summary, a simple method for the fabrication of a magnetic mesoporous SBA-15/IBU delivery system has been described. These materials not only possessed large surface area, high pore volume and large pore size, but also had well superparamagnetism. The magnetic iron oxide nanoparticles of Fe₂O₃/SBA-15/IBU made the material conductible in an external magnetic field. Moreover, the Fe₂O₃/SBA-15/IBU delivery system exhibited well control release ability in SIF because of the stronger interaction between the drug molecule and the host. From the above investigation, the magnetic mesoporous materials have shown ‘smart’ drug carrier capacity of magnetic oriented and alkalescence site target release.

Acknowledgements

Financial support for this study was provided by the Foundation of Harbin Educational Committee (12521164).

References

1. J. Kim, H. S. Kim, N. Lee, T. Kim, H. Kim, T. Yu, I. C. Song, W. K. Moon and T. Hyeon: *Angew. Chem. Int. Ed.*, 2008, **47**, 8438.
2. C. P. Tsai, Y. Hung, Y. H. Chou, D. M. Huang, J. K. Hsiao, C. Chang, Y. C. Chen and C. Y. Mou: *Small*, 2008, **4**, 186.
3. Y. S. Lin, S. H. Wu, Y. Hung, Y. H. Chou, C. Chang, M. L. Lin, C. P. Tsai and C. Y. Mou: *Chem. Mater.*, 2006, **18**, 5170.
4. K. M. L. Taylor, J. S. Kim, W. J. Rieter, H. An, W. L. Lin and W. B. Lin: *J. Am. Chem. Soc.*, 2008, **130**, 2154.
5. D. M. Huang, Y. Hung, B. S. Ko, S. C. Hsu, W. H. Chen, C. L. Chien, C. P. Tsai, C. T. Kuo, J. C. Kang, C. S. Yang, C. Y. Mou and Y. C. Chen: *FASEB J.*, 2005, **19**, 2014.
6. F. Y. Qu, G. S. Zhu, H. M. Lin, W. W. Zhang, J. Y. Sun, S. G. Li and S. L. Qiu: *J. Solid State Chem.*, 2006, **179**, 2027.
7. I. I. Slowing, B. G. Trewyn and V. S. Y. Lin: *J. Am. Chem. Soc.*, 2007, **129**, 8845.
8. J. Lu, M. Liong, J. I. Zink and F. Tamanoi: *Small*, 2007, **3**, 1341.
9. D. R. Radu, C. Y. Lai, K. Jeftinija, E. W. Rowe, S. Jeftinija and V. S. Y. Lin: *J. Am. Chem. Soc.*, 2004, **126**, 13216.
10. F. Torney, B. G. Trewyn, V. S. Y. Lin and K. Wang: *Nat. Nanotechnol.*, 2007, **2**, 295.
11. M. Vallet-Regí, F. Balas and D. Arcos: *Angew. Chem. Int. Ed.*, 2007, **46**, 7548.
12. W. J. Xu, Q. Gao and Y. Xu: *Mater. Res. Bull.*, 2009, **44**, 606.
13. C. Y. Liu, J. Guo and W. L. Yang: *J. Mater. Chem.*, 2009, **19**, 4764.
14. H. M. Lin, W. K. Wang, P. A. Hsiung and S. G. Shyu: *Acta Biomater.*, 2010, **6**, 3256.
15. S. M. Zhu, D. Zhang and Z. X. Chen: *J. Mater. Chem.*, 2009, **19**, 7710.
16. Y. F. Zhu, E. Kockrick and T. Ikoma: *Chem. Mater.*, 2009, **21**, 2547.
17. B. Liu, X. L. Yang and H. F. Ji: *Polym. Int.*, 2010, **59**, 961.
18. T. Valdés-Solis, A. F. Rebollo and M. Sevilla: *Chem. Mater.*, 2009, **21**, 1806.
19. D. Y. Zhao, J. L. Feng, Q. S. Huo, N. Melosh, G. H. Fredrickson, B. F. Chmelka and G. D. Stucky: *Science*, 1998, **279**, 548.
20. D. Y. Zhao, Q. S. Huo, J. L. Feng, B. F. Chmelka and G. D. Stucky: *J. Am. Chem. Soc.*, 1998, **120**, 6024.
21. M. Kruk, M. Jaroniec, C. H. Ko and R. Ryoo: *Chem. Mater.*, 2000, **12**, 1961.
22. H. F. Yang, Q. H. Shi, B. Z. Tian, S. H. Xie, F. Q. Zhang, Y. Yan, B. Tu and D. Y. Zhao: *Chem. Mater.*, 2003, **15**, 536.
23. F. Siewmann, J. Siewmann, M. Walther, R. J. MacRae and R. Bodmeier: *J. Controlled Release*, 2005, **105**, 226.
24. M. Grun, K. K. Unger, A. Matsumoto and K. Tsutsumi: *Microporous Mesoporous Mater.*, 1999, **27**, 207.
25. Q. A. Pankhurst, J. Connolly, S. K. Jones and J. Dobson: *J. Phys. D: Appl. Phys.*, 2003, **36D**, 167.
26. J. E. Bateman, R. D. Eagling, D. R. Worrall, B. R. Horrocks: *Angew. Chem. Int. Ed.*, 1998, **37**, 2683.